ChemComm

ROYAL SOCIETY OF CHEMISTRY

COMMUNICATION

View Article Online
View Journal | View Issue

Open Access Article. Published on 22 July 2024. Downloaded on 10/27/2025 8:58:16 AM.
This article is licensed under a Creative Commons Attribution 3.0 Unported Licence.

Check for updates

Cite this: *Chem. Commun.*, 2024, **60**, 8744

Received 9th April 2024,
Accepted 19th July 2024

DOI: 10.1039/d4cc01572j

rsc.li/chemcomm

A dual DNA-binding conjugate that selectively recognizes G-quadruplex structures†

Mitsuharu Ooga,[a] Vinodh J. Sahayasheela,[a] Yuki Hirose,[a] Daisuke Sasaki,[a] Kaori Hashiya,[a] Toshikazu Bando*[a] and Hiroshi Sugiyama*[b]

G-quadruplex (G4) structures play roles in various biological processes, but the challenge lies in specific targeting. To address this, we synthesized a conjugate capable of recognizing the G4 structure and its proximal duplex. Our conjugate can enable recognition of specific G4s in the human genome to understand and target those structures.

Nucleic acids are known to form structures apart from the canonical Watson–Crick double-helix.[1] Among them, G-quadruplexes (G4s) are well-known secondary structures that arise from guanine-rich sequences through stacked G tetrads by Hoogsteen hydrogen bonding and are further stabilized by monovalent cations (K^+, Na^+) between the tetrad.[2] G4 structures arising from the telomere repeat sequences and oncogene promoter regions are thought to play important biological roles in the processing of telomere-ends[3] and the regulation of gene expression, respectively.[4] Therefore, various small molecules have been developed to stabilize the G4 structure, making it a promising drug target.[5–7] However, the genome-wide analysis using a G4 ligand identified more than 700 000 G4-forming sequences,[8] and targeting a specific G4-forming sequence still remains a challenge given the topological similarity among diverse G4-forming sequences.

A promising approach to overcome this challenge is the simultaneous recognition of both G4 and its proximal DNA regions. Earlier using this approach our lab[9,10] and other groups[11,12] were able to achieve success in obtaining G4 selectivity. With the advancement of G4-mapping techniques[13] and reports of crystal structures of a G4-duplex complex,[14,15] it is possible to design molecules that can recognize both G4 and its proximal DNA regions to reveal its function by selective targeting. More recently, while this manuscript was under preparation, the G4 ligand conjugated with oligonucleotide was also reported.[16]

However, to achieve a higher-level recognition retaining affinity towards a selective G4 site for biological studies, it is necessary to identify diverse candidates. Herein, we synthesized a conjugate consisting of a PyPDS, a well-known G4 ligand,[17,18] and pyrrole–imidazole polyamide (PIP), a programmable sequence-specific DNA minor-groove binder.[19,20] We demonstrated the selective G4 recognition of the conjugate, thereby illustrating its potential as a tool to delineate the function of selective G4 structures and target them.

To investigate the binding ability and sequence selectivity, we chose the c-MYC G4 forming region and its adjacent duplex sequence in the nuclease hypersensitive element (NHE) III_1 as a dual-target (Fig. S1, ESI†). PIPs **1** and **2** (Fig. 1a) targeting the flanking region proximal to G4 in the c-MYC promoter were utilized as the duplex binder. The PIPs obtained by solid-phase synthesis were conjugated with PyPDS *via* linkers to produce conjugates **1**–**3** (Fig. 1b and Schemes S1–S3, ESI†). Conjugates **1** and **2** were designed using PIP **1**, whereas conjugate **3** was designed using PIP **2**.

To evaluate whether the hybrid molecules could maintain their G4-stabilizing effect on the c-MYC quadruplex, we

Table 1 DNA sequences. Nucleotides in bold represent G4-forming sequences, those in bold and italics represent PIP recognition sites and those in red represent changes from the target sequence

Target	5′-A**GGGTGGGTAGGGTGGGT**A***AGGTG***CG-3′
	3′-A***TTCCAC***GC-5′
Non-target	5′-A**GGGTGGGTAGGGTGGGT**A**AT*TTG***CG-3′
	3′-A***TTAAAC***GC-5′
Non-G4	5′-A**AAAT**A**AAT**A**AAAT**A**AAT**A***AGGTG***CG-3′
	3′-A***TTCCAC***GC-5′
G4	5′-A**GGGTGGGTAGGGTGGG**-3′
ds	5′-T***AAGGTG***CG-3′
	3′-A***TTCCAC***GC-5′

[a] Department of Chemistry, Graduate School of Science, Kyoto University, Kitashirakawa-Oiwakecho, Sakyo-ku, Kyoto 606-8502, Japan. E-mail: bando@kuchem.kyoto-u.ac.jp

[b] Institute for Integrated Cell-Material Sciences (iCeMS), Kyoto University, Yoshida-ushinomiyacho, Sakyo-ku, Kyoto 606-8501, Japan. E-mail: hs@kuchem.kyoto-u.ac.jp

† Electronic supplementary information (ESI) available. See DOI: https://doi.org/10.1039/d4cc01572j

This journal is © The Royal Society of Chemistry 2024

Open Access Article. Published on 22 July 2024. Downloaded on 10/27/2025 8:58:16 AM.
This article is licensed under a Creative Commons Attribution 3.0 Unported Licence.

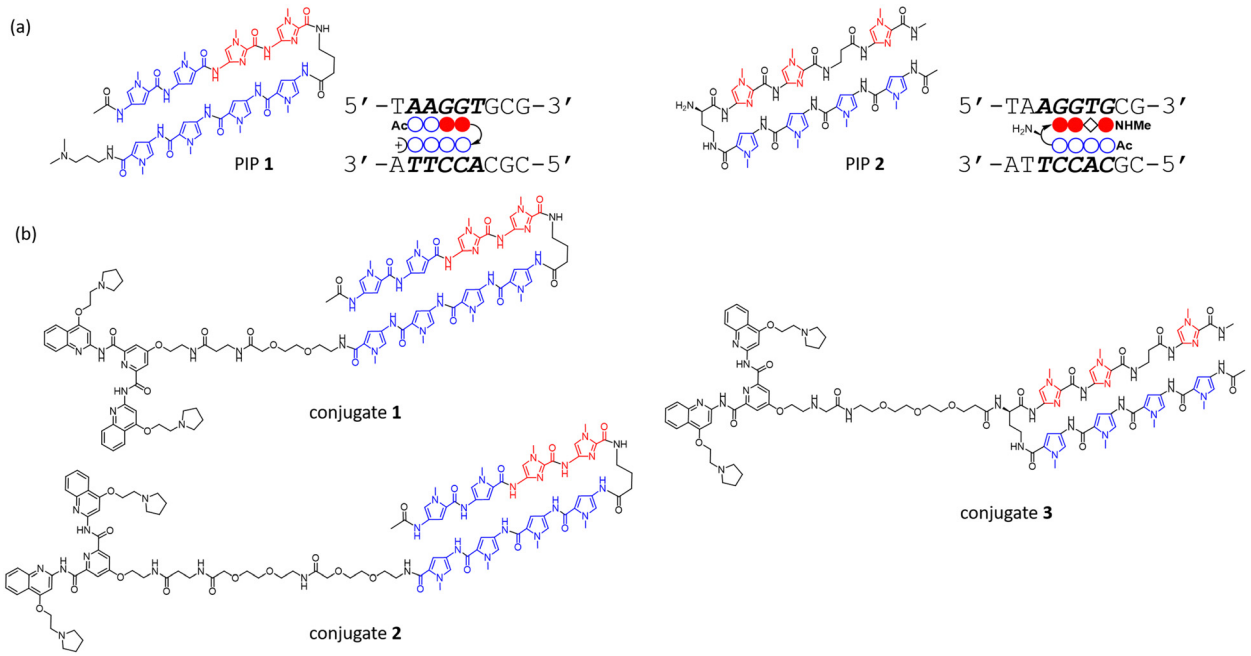

Fig. 1 (a) Chemical structures and ball-and-stick notations of PIPs **1** and **2** and their recognition sequences; the blue circles, red-filled circles, and black diamonds represent *N*-methylpyrrole, *N*-methylimidazole, and β-alanine residues, respectively. The curved line connecting the sides of two circles represents γ-aminobutyric acid. The plus sign of PIP **1** represents an *N*,*N*-dimethyl-1,3-propandiamine (Dp) residue. (b) Chemical structures of conjugates **1**–**3**.

monitored the thermal denaturing profiles of the G4 formation using circular dichroism (CD) in the presence or absence of the hybrid compounds. We utilized the target DNA sequence with G-to-T modifications at the G4-duplex interface to facilitate the formation of G4 and prevent the alternative hybridization of the shorter strand based on our previous research[9] (Table 1). The CD spectrum of the target DNA showed combined signals derived from both G4 and B-form structures (Fig. S2a, ESI,† and Table 1). To accurately measure the melting temperature from the G4 structures alone, it is necessary to use a wavelength where the duplex effect is minimal. From our previous study using hairpin duplex DNA segments,[9] we found that 267 nm was the ideal wavelength for measuring the signal derived from the G4 structure. To validate this, the signal of the duplex segment at that specific wavelength was measured, and the results revealed little change (Fig. S3, ESI†), indicating that the duplex region had minimal impact on the target sequence at this wavelength. Moving forward, the signal at 267 nm was measured to obtain the melting curves of the G4 moiety in the presence or absence of each compound (Fig. 2 and Fig. S4, ESI†). The melting curves indicated that all the conjugates stabilized the G4 structure, and from the comparison of the

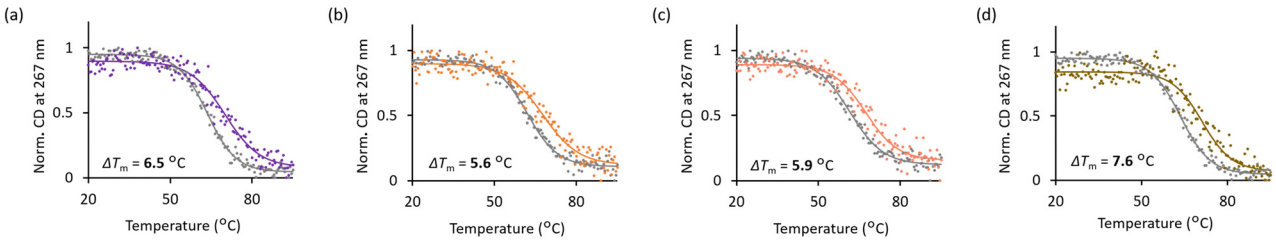

Fig. 2 Normalized CD melting curves for the target (G4-duplex chimera) sequence (5 μM) in the absence (gray) or presence of 1 molar equivalent of compounds (colored): (a) PyPDS; (b) conjugate **1**; (c) conjugate **2**; and (d) conjugate **3**.

Table 2 Changes in the duplex melting temperature values (ΔT_m) of the target sequence (2.5 μM) in the presence of compounds (3 molar equivalents) detected by absorbance at 260 nm

	PyPDS	PIP **1**	Conjugate **1**	Conjugate **2**	PIP **2**	Conjugate **3**
ΔT_m [°C]	11.0 ± 0.3	0.4 ± 0.3	17.2 ± 0.4	16.8 ± 0.6	24.3 ± 0.5	26.8 ± 0.3

Open Access Article. Published on 22 July 2024. Downloaded on 10/27/2025 8:58:16 AM.
This article is licensed under a Creative Commons Attribution 3.0 Unported Licence.

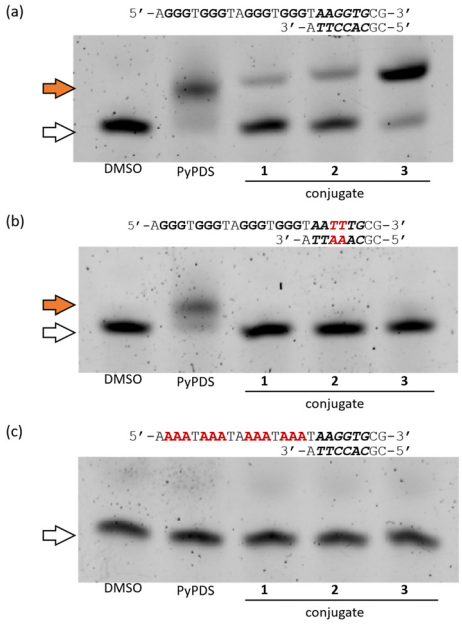

Fig. 3 Native gel electrophoresis for comparing the binding preference of compounds (5 molar equivalents) towards (a) the target sequence; (b) the non-target sequence; and (c) the non-G4 sequence. Orange and white arrows indicate the bands of the DNA–compound complex and DNA alone, respectively.

melting temperature increase (ΔT_m), conjugate **3** showed higher values (ΔT_m = 7.6 °C) than the other two conjugates. Interestingly, conjugate **3** also showed better G4 stabilizing ability than PyPDS alone (ΔT_m = 6.5 °C) under the condition in which one equivalent of the compound was added to DNA. These results validate that the conjugates were able to stabilize the G4 structures comparable to PyPDS.

Next, the stabilization of the duplex region by the hybrid compounds was evaluated through UV melting assays. The absorption-based melting curve of the target DNA segment detected at 260 nm revealed two inflection points and it was estimated to undergo melting in the following order: (i) the duplex and (ii) the G4 structure (Fig. S5a, ESI†). To clarify the inflection point corresponding to duplex melting, several validations were carried out. First, the CD signals of the target DNA and the DNA lacking the complementary strand of the duplex region were measured (Fig. S5b, ESI†). Measurements using CD melting at 10 °C and 55 °C revealed that the CD signals were very similar in both DNA sequences, suggesting that the duplex signal largely disappeared from the CD signal of the target DNA (Fig. S5b and c, ESI†). Additionally, a comparison of CD spectra in the presence or absence of the conjugates at 10 °C and 55 °C showed that the signal derived from parallel G4 remained, while the signal derived from PIP binding in the minor groove (330 nm) disappeared with increasing temperature (Fig. S6, ESI†). These results indicated that the increase in absorbance from 10 to 55 °C was largely due to the dissociation of the duplex region, and the binding of PIP towards the target sequence increased the melting temperature. Note that the addition of PyPDS had no substantial impact on the waveform

Table 3 DC_{50} values for the target and non-target sequences determined by the ThT displacement assay. *S* is the ratio determined by DC_{50} for the non-target sequence/DC_{50} for the target sequence and indicates G4 selectivity for the target sequence over the non-target sequence

	DC_{50} [μM]		
	Target	Non-target	*S*
PyPDS	0.54	0.56	1.0
Conjugate **1**	1.1	2.1	1.9
Conjugate **2**	1.2	2.0	1.7
Conjugate **3**	0.88	2.0	2.3

Table 4 DC_{50} values for the target and non-target sequences determined by the EtBr displacement assay. *S* is the ratio determined by DC_{50} for the non-target sequence/DC_{50} for the target sequence and indicates duplex selectivity for the target sequence over the non-target sequence

	DC_{50} [μM]		
	Target	Non-target	*S*
PyPDS	2.1	1.4	0.67
Conjugate **1**	1.8	3.5	1.9
Conjugate **2**	1.5	3.4	2.3
Conjugate **3**	1.3	2.9	2.2

of the CD spectrum of the target DNA, and similarly to other G4-stabilizing ligands, a slight decrease in G4-derived signals, such as those at 260 and 240 nm, was also detected[21] (Fig. S7, ESI†).

To assess the thermal stability of the conjugates to their target duplex region, we calculated the positive shifts of the melting temperature by the addition of compounds (Table 2 and Fig. S8, ESI†). The increased ΔT_m values of the conjugates compared to PIP or PyPDS alone confirmed their enhanced double-strand stabilizing ability. The slightly higher ΔT_m values for conjugate **3** (ΔT_m = 26.8 °C) compared to PIP **2** (ΔT_m = 24.3 °C) could be attributed to the high ΔT_m values of PIP **2** itself. The stabilization of the double-stranded DNA by PyPDS (ΔT_m = 11.0 °C) may be likely due to its binding in the region between G4 and the duplex segment and indeed a NMR-based model of PyPDS binding at the interface of the G-quartet and the double-stranded loop structure has been reported.[22] Additionally, we performed the FRET melting assay utilizing DNA oligomers labeled with a fluorescein and a tetramethylrhodamine at the opposite end of G4 (Fig. S9a, ESI†). This method also demonstrated the duplex stabilizing ability of the conjugates, and the order of the ΔT_m values was consistent with that of UV melting at 260 nm, except for a reversal due to a slight difference between conjugates **1** and **2** (Table S1 and Fig. S9b–g, ESI†).

The results of the melting studies demonstrated that the conjugates were capable of stabilizing both the G4 and duplex regions of the target DNA, indicating their dual recognition abilities. In sum, conjugate **3** exhibited high thermal stability in both G4 and duplex regions. The energy-minimized structure of the DNA–conjugate **3** complex suggested a binding model in which the PyPDS moiety was inserted between the G4 and duplex regions (Fig. S10, ESI†).

To investigate the selectivity of the conjugates, we performed native gel electrophoretic mobility shift assays (EMSA) using

 This journal is © The Royal Society of Chemistry 2024

Open Access Article. Published on 22 July 2024. Downloaded on 10/27/2025 8:58:16 AM.
This article is licensed under a Creative Commons Attribution 3.0 Unported Licence.

the target DNA sequence, the non-target DNA sequence, and the non-G4 DNA sequence (Fig. 3 and Fig. S11, ESI†). The DNA sequences used in this assay were initially confirmed to form G4 structures by CD spectrometry (Fig. S2, ESI†). As shown in Fig. 3a, in the case of the target DNA sequence, all conjugates including PyPDS showed an upward shift of the DNA band, with the intensity of the upshifted bands in the order of conjugate **1** < **2** < **3**. The increase in band intensity by conjugate **3** from our EMSA can be explained by its high thermal stability demonstrated from our melting experiments. In contrast, in the presence of the non-target DNA sequence, only PyPDS showed a band shift, validating the selective binding of the conjugates to the target sequence alone (Fig. 3b). Finally, the conjugates showed no band shift with the non-G4 forming sequence containing duplex binding sites (Fig. 3c). Taken together, our EMSA assays indicate that efficient binding of conjugates requires the presence of both G4 and target duplex regions.

To further assess the selectivity of conjugates, fluorescent indicator displacement assays using thioflavin T (ThT) or ethidium bromide (EtBr) were carried out. ThT is a fluorescent probe that emits enhanced fluorescence upon binding to G4 structures, and its fluorescence intensity decreases upon displacement by G4 ligands, allowing for the identification of selective G4 binding compounds.[23,24] We first confirmed that ThT showed enhanced fluorescence intensity when bound to the different G4 sequences, including the dual binding sites compared to double-stranded or non-G4 forming sequences. Additionally, EtBr, a commonly used fluorescent probe for double-stranded DNA, showed enhanced fluorescence when bound to DNA sequences containing duplex regions, compared to G4-only sequences (Fig. S12, ESI,† and Table 1). By using target and non-target DNA sequences, we then examined the concentration-dependent displacement of ThT or EtBr by each compound, resulting in the generation of displacement curves (Fig. S13 and S14, ESI†). The evaluation of the binding ability of the compounds was based on the DC_{50} value, which is the concentration required to displace 50% of the fluorescent indicator.[25] With the DC_{50} values for both DNA sequences, the S value (DC_{50} for the non-target sequence/DC_{50} for the target sequence) was calculated as the measure of selectivity. For the ThT displacement assay, which evaluated G4 binding, PyPDS showed a value of 1 for the S value, indicating no difference between the sequences. In contrast, all conjugates had S values greater than 1, indicating preferential binding to the target sequences (Table 3) and conjugate **3** had the highest value (S = 2.3). The use of EtBr as a double-stranded fluorescent indicator demonstrated that the displacement rate for PyPDS reached saturation at 60%, with an S value of 0.67 (Fig. S14a, ESI,† and Table 4). In contrast, the S value for conjugates was above 1. These results suggest that the selectivity of the duplex region in conjugates contributes to the selectivity of G4.

In summary, the PyPDS–PIP hybrid compounds we developed exhibit the ability to recognize both G4 and its proximal duplex regions concurrently. This allows for the selective recognition of a specific G4, thereby suggesting that the conjugation of G4 ligands with PIP could be an effective strategy for designing ligands targeting specific G4-forming sequences. In the future, we will test our approach to visualize and modulate selective G4 structures for biological application.

Data availability

The data supporting this article have been included as part of the ESI.†

Conflicts of interest

There are no conflicts to declare.

Notes and references

1 J. Choi and T. Majima, *Chem. Soc. Rev.*, 2011, **40**, 5893–5909.
2 D. Varshney, J. Spiegel, K. Zyner, D. Tannahill and S. Balasubramanian, *Nat. Rev. Mol. Cell Biol.*, 2020, **21**, 459–474.
3 H. J. Lipps and D. Rhodes, *Trends Cell Biol.*, 2009, **19**, 414–422.
4 T. Tian, Y.-Q. Chen, S.-R. Wang and X. Zhou, *Chemistry*, 2018, **4**, 1314–1344.
5 N. Kosiol, S. Juranek, P. Brossart, A. Heine and K. Paeschke, *Mol. Cancer*, 2021, **20**, 40.
6 S. Asamitsu, S. Obata, Z. Yu, T. Bando and H. Sugiyama, *Molecules*, 2019, **24**, 429.
7 Y. Ma, K. Iida and K. Nagasawa, *Biochem. Biophys. Res. Commun.*, 2020, **531**, 3–17.
8 V. S. Chambers, G. Marsico, J. M. Boutell, M. Di Antonio, G. P. Smith and S. Balasubramanian, *Nat. Biotechnol.*, 2015, **33**, 877–881.
9 S. Asamitsu, S. Obata, A. T. Phan, K. Hashiya, T. Bando and H. Sugiyama, *Chemistry*, 2018, **24**, 4428–4435.
10 S. Mandal, Y. Kawamoto, Z. Yue, K. Hashiya, Y. Cui, T. Bando, S. Pandey, M. E. Hoque, M. A. Hossain, H. Sugiyama and H. Mao, *Nucleic Acids Res.*, 2019, **47**, 3295–3305.
11 E. Cadoni, L. De Paepe, G. Colpaert, R. Tack, D. Waegeman, A. Manicardi and A. Madder, *Nucleic Acids Res.*, 2023, **51**, 4112–4125.
12 J.-H. Yuan, J.-L. Tu, G.-C. Liu, X.-C. Chen, Z.-S. Huang, S.-B. Chen and J.-H. Tan, *Nucleic Acids Res.*, 2022, **50**, 4246–4257.
13 S. Galli, G. Flint, L. Růžičková and M. Di Antonio, *RSC Chem. Biol.*, 2024, **5**, 426–438.
14 I. Russo Krauss, S. Ramaswamy, S. Neidle, S. Haider and G. N. Parkinson, *J. Am. Chem. Soc.*, 2016, **138**, 1226–1233.
15 R. C. Monsen, E. Y. D. Chua, J. B. Hopkins, J. B. Chaires and J. O. Trent, *Nucleic Acids Res.*, 2023, **51**, 1943–1959.
16 A. Berner, R. N. Das, N. Bhuma, J. Golebiewska, A. Abrahamsson, M. Andréasson, N. Chaudhari, M. Doimo, P. P. Bose, K. Chand, R. Strömberg, S. Wanrooij and E. Chorell, *J. Am. Chem. Soc.*, 2024, **146**, 6926–6935.
17 S. Müller, D. A. Sanders, M. Di Antonio, S. Matsis, J.-F. Riou, R. Rodriguez and S. Balasubramanian, *Org. Biomol. Chem.*, 2012, **10**, 6537–6546.
18 M. Di Antonio, A. Ponjavic, A. Radzevičius, R. T. Ranasinghe, M. Catalano, X. Zhang, J. Shen, L.-M. Needham, S. F. Lee, D. Klenerman and S. Balasubramanian, *Nat. Chem.*, 2020, **12**, 832–837.
19 C. L. Kielkopf, E. E. Baird, P. B. Dervan and D. C. Rees, *Nat. Struct. Biol.*, 1998, **5**, 104–109.
20 P. B. Dervan and B. S. Edelson, *Curr. Opin. Struct. Biol.*, 2003, **13**, 284–299.
21 E. Palma, C. Içhedef, C. Fernandes, A. Belchior, P. Raposinho, L. Gano, A. Miranda, D. Moreira, P. Lourenço, C. Cruz, A. S. Pires, M. F. Botelho and A. Paulo, *Chem. – Eur. J.*, 2024, **30**, e202400285.
22 L.-Y. Liu, T.-Z. Ma, Y.-L. Zeng, W. Liu and Z.-W. Mao, *J. Am. Chem. Soc.*, 2022, **144**, 11878–11887.
23 A. Renaud de la Faverie, A. Guédin, A. Bedrat, L. A. Yatsunyk and J.-L. Mergny, *Nucleic Acids Res.*, 2014, **42**, e65.
24 J. Jamroskovic, M. Livendahl, J. Eriksson, E. Chorell and N. Sabouri, *Chemistry*, 2016, **22**, 18932–18943.
25 D. Monchaud and M.-P. Teulade-Fichou, *Methods Mol. Biol.*, 2010, **608**, 257–271.